J. Fluid Mech. (1981), *vol.* 108, *pp.* 273–289
Printed in Great Britain

Convection in an imposed magnetic field. Part 2. The dynamical regime

By N. O. WEISS

Department of Applied Mathematics and Theoretical Physics,
University of Cambridge

(Received 29 July 1980)

Nonlinear, two-dimensional magnetoconvection has been investigated numerically for a fixed Rayleigh number of 10^4, with the ratio ζ of the magnetic to the thermal diffusivity in the range $0{\cdot}4 \geqslant \zeta \geqslant 0{\cdot}05$. As the Chandrasekhar number Q is decreased, convection first sets in as overstable oscillations, which are succeeded by steady convection with dynamically active flux sheets and, eventually, with kinematically concentrated fields. In the dynamical regime spatially asymmetrical convection, with most of the flux on one side of the cell, is preferred. As Q increases, these asymmetrical solutions become time-dependent, with oscillations about the steady state which develop into large-scale oscillations with reversals of the flow. Although linear theory predicts that narrow cells should be most unstable, the nonlinear results show that steady convection occurs most easily in cells that are roughly twice as wide as they are deep.

1. Introduction

The Sun is the only star on which magnetic fields can be observed in any detail and the most striking feature of solar magnetic fields is that they are confined to isolated flux tubes. Nearly all the magnetic flux that emerges through the sun's surface outside active regions is compressed into slender ropes, with intense magnetic fields, which nestle between the granular convection cells. On a larger scale, active regions display a similar intermittent structure. In order to explain this behaviour it is natural to begin by studying the effect of convection on an externally imposed magnetic field in a layer heated uniformly from below.

This paper presents some results of numerical experiments on an idealized, two-dimensional model of nonlinear magnetoconvection in a Boussinesq fluid. These calculations cover the entire range from a kinematic regime, where the fields are sufficiently weak for the Lorentz force to be neglected, to fields that are strong enough to suppress convection altogether. In particular, it is possible to explore the transition from the kinematic to the dynamical regime and to study different aspect ratios and planforms for convection. Many features found in this two-dimensional geometry occur also in the axisymmetric system that was investigated by Galloway & Moore (1979).

Part 1 (Weiss 1981*a*, hereafter referred to as I) was concerned with the pattern of bifurcation from the static solution and the connection between small-amplitude theory and nonlinear convection. For this purpose, the Rayleigh number R was increased while the Chandrasekhar number Q was held fixed; this corresponded to

raising the temperature gradient with a constant mean magnetic field $\mathbf{B}_0$. For this paper it is more appropriate to regard the temperature gradient as fixed and to investigate the effect of increasing B_0; hence Q will be varied while R remains constant. This procedure is computationally more convenient too, since R can be chosen to ensure adequate resolution in the kinematic regime. The results in these two papers can be related by remembering that increasing R is roughly equivalent to decreasing Q and vice versa.

When the ratio, ζ, of the magnetic to the thermal diffusivity is sufficiently small convection first sets in, as Q is decreased, as overstable oscillations at $Q = Q^{(o)}$. Steady convection is possible for $Q < Q_{\max}$ and the transformation from a dynamical to a kinematic regime occurs when $Q = Q_m$, so that $Q_m < Q_{\max} < Q^{(o)}$ when R is sufficiently large. The full dynamic range will be explored for a moderate value of the Rayleigh number, $R = 10^4$, and $0{\cdot}1 \leqslant \zeta \leqslant 1$. The results in Part I implied that $Q_{\max} \sim R/\zeta$ (cf. Cowling 1976) and the transition from a kinematic to a dynamical region has already been investigated numerically for the simpler Oberbeck problem (Peckover & Weiss 1978) and analysed by Galloway, Proctor & Weiss (1978). This transition occurs as the field becomes strong enough to exclude motion from the sheets to which magnetic flux has been confined, so that $Q_m \sim \zeta^{-\frac{1}{2}} R^{\frac{1}{2}}$ (Galloway *et al.* 1978). At the same time the field in the flux sheets reaches its maximum value B_m: the numerical results in §2 confirm that $B_m \propto \zeta^{-0{\cdot}2}$ (Peckover & Weiss 1978).

The equations governing two-dimensional magnetoconvection were derived in I and will not be repeated here. The next section presents results covering the full dynamical regime for $R = 10^4$ and including the transition at Q_m. In these runs, two similar flux sheets are formed symmetrically on either side of a cell. Section 3 investigates an alternative family of solutions, with most of the flux concentrated into a larger sheet on one side or the other, while the convective eddy occupies the rest of the cell. Although these spatially asymmetrical solutions transport slightly less heat than the symmetrical cells, they seem to be preferred throughout the dynamical regime. As Q is increased, convection becomes time-dependent: initially there are oscillations about the steady state without reversing the main flow; subsequently these develop into full-scale oscillations, whose asymmetry diminishes as Q approaches $Q^{(o)}$. For large R, linear theory implies that $Q^{(o)}$ should be greatest for cells that are elongated parallel to the field, so that the ratio, λ, of the cell width to its depth is small. When $R = 10^4$ there is no tendency for square cells to split, but the results in §4 show that $Q_{\max}$ is much greater for $\lambda = 2$ than for $\lambda = 1$: in the nonlinear regime, flat cells are apparently preferred. The paper concludes with an attempt to relate these theoretical results to the intermittent structure of magnetic fields in the sun. The model treated here is highly idealized but it does shed some light on the behaviour of turbulent magnetic fields.

2. The transition from a dynamical to a kinematic regime

The model problem is described in I. A particular configuration is specified by five dimensionless parameters. These are the Rayleigh number R, the Chandrasekhar number Q and the Prandtl numbers σ and ζ, which are defined in equations I(2.9)–I(2.11) (where the prefix I refers to the paper I), together with the dimensionless cell width λ. Nonlinear behaviour is governed by the partial differential equations

ζ	$Q^{(o)}$	$Q^{(i)}$	$Q^{(e)}$	$Q_{\max}$
1	—	—	467	—
0·4	1533	635	467	—
0·2	3748	1055	467	1050
0·1	8343	1920	467	2100
0·05	17641	3661	467	—

TABLE 1. Runs with $R = 10^4$, $\lambda = 1$.

I(2.12)–I(2.15), which are solved numerically in the region $\{0 < x < \lambda;\ 0 < z < 1\}$, subject to the boundary conditions I(2.16)–I(2.18). The results of linear perturbation theory are summarized in §3 of I. It will, however, prove convenient to rewrite these expressions so as to provide explicit formulae for critical values of Q when R is regarded as fixed. Provided that $R > R_0 = \pi^4(1+\lambda^2)^3/\lambda^4$, there is a simple bifurcation from the static solution (corresponding to a marginal state) at $Q = Q^{(e)}$, where

$$Q^{(e)} = (R - R_0)/[\pi^2(1+\lambda^2)], \tag{2.1}$$

from I(3.3). If $\zeta < 1$ and

$$R > [\zeta^2(\sigma+\zeta)/\{\sigma(1-\zeta)\}]R_0, \tag{2.2}$$

the simple bifurcation is preceded by a Hopf bifurcation (the onset of overstability) at $Q = Q^{(o)}$, where

$$Q^{(o)} = \frac{1}{\pi^2(1+\lambda^2)}\frac{(1+\sigma)}{\zeta(\sigma+\zeta)}\left[R - \frac{(1+\zeta)(\sigma+\zeta)}{\sigma}R_0\right], \tag{2.3}$$

from I(3.6). There is a pair of complex conjugate eigenvalues (corresponding to the presence of overstable oscillations) for the range $Q^{(o)} \geqslant Q \geqslant Q^{(i)}$. At $Q^{(i)}$ there is a transition to real eigenvalues (corresponding to monotonic, or direct, unstable modes) one of which passes through zero at $Q^{(e)}$. Thus $Q^{(e)} < Q^{(i)} < Q^{(o)}$ if (2.2) is satisfied. The value of $Q^{(i)}$ can be found by solving a cubic equation; for all the cases considered in this paper $\sigma = 1$ and the cubic reduces to

$$(q_1 - 1)^3 + r_1[(2 - r_1) + 5q_1 - \tfrac{1}{4}q_1^2] = 0, \tag{2.4}$$

cf. I(3.8), where

$$q_1 = \pi^2(1+\lambda^2)\zeta Q/R, \quad r_1 = (1-\zeta)^2 R_0/R. \tag{2.5}$$

For all the nonlinear results in §2 and §3 of this paper, $R = 10^4$ and $\lambda = 1$ (corresponding to square cells). Hence $R/R_0 \approx 12{\cdot}83$ and overstability is possible for $\zeta < 0{\cdot}885$. Runs were made with $0{\cdot}05 \leqslant \zeta \leqslant 1$; the corresponding values of $Q^{(o)}$, $Q^{(i)}$ and $Q^{(e)}$ are listed in table 1. Details of these runs, and of all others used in this paper, are specified in the appendix. The full dynamical range was investigated for $\zeta = 0{\cdot}2$ and $0{\cdot}1$ and figure 1 shows the variation with Q of the Nusselt number N, defined in I(4.3). This figure should be compared with figure 3 of I: decreasing Q has an effect qualitatively similar to that of increasing R but for small Q the Nusselt number tends asymptotically to the value that it would have in the absence of any magnetic field. Finite-amplitude oscillations were found for $Q < Q^{(o)}$; both the maximum value of N, $N_{\max}$, and the time-averaged value, $\overline{N}$, are shown in figure 1. As Q decreases, $N_{\max}$ first rises and then drops as Q approaches $Q_{\max}$, the highest value

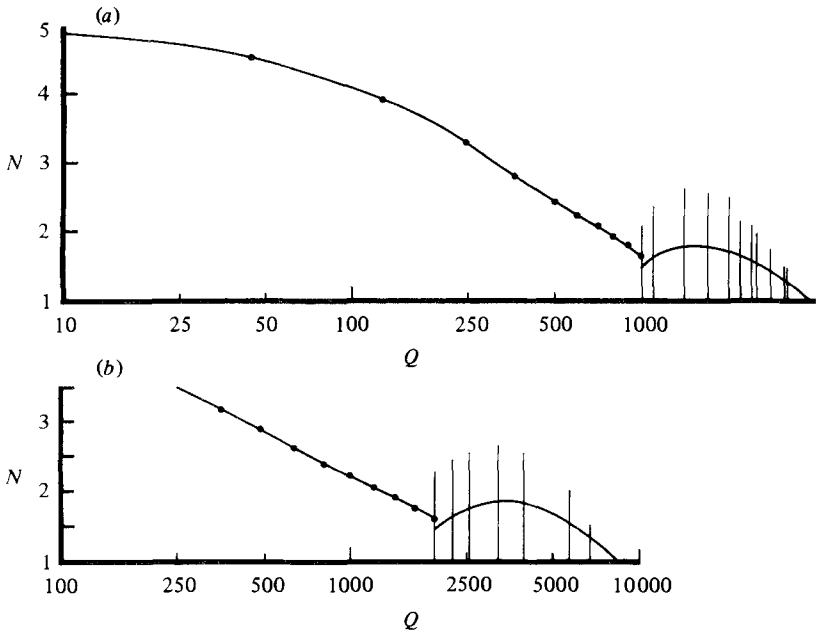

FIGURE 1. The dynamical range: variation of the Nusselt number N with Q for $R = 10^4$, $\lambda = 1$ and (*a*) $\zeta = 0{\cdot}2$, (*b*) $\zeta = 0{\cdot}1$. The continuous lines indicate values of N for steady solutions and time-averaged values for oscillatory solutions; the vertical bars show the maximum amplitudes of oscillatory solutions.

of Q for which steady convection can occur. $\overline{N}$ behaves similarly and when $Q = Q_{\max}$ the value of $\overline{N}$ is slightly less than the value of N for the steady solution. For $Q < Q_{\max}$, N varies smoothly and no sharp transition between the dynamical and kinematic regimes can be detected in figure 1.

This transition can, however, be located by inspecting the amplified field in the flux sheets. It is convenient to introduce the dimensionless Alfvén speed $V_0 = (\sigma\zeta Q)^{\frac{1}{2}}$ as a measure of the imposed magnetic field and to describe the amplified field by $V^* = (\sigma\zeta Q)^{\frac{1}{2}} B^*$, where B^* is the peak value of the dimensionless field in the flux sheets. In figure 2(*a*), V^* is plotted against V_0. (In dimensional terms this is equivalent to plotting B^* against B_0.) For $\zeta = 0{\cdot}2$, the field is amplified by a factor close to 4 when $Q = Q_{\max}$. Then as V_0 decreases the amplified field continues to rise until it reaches a maximum, with $B^* \approx 9$. Thereafter the amplified field falls and eventually enters an asymptotic regime where $V^* \propto V_0$ ($B^* \approx 15$). This is the kinematic regime that was described in § 3 of I. If U is the maximum value of $|w|$ then we can define the magnetic Reynolds number $R_m = U/\zeta$ and we expect that $B^* \propto R_m^{\frac{1}{2}}$ in the kinematic regime. From the numerical results we find that $B^* \approx 1{\cdot}2R_m^{\frac{1}{2}}$ for this particular configuration (cf. Peckover & Weiss 1978).

The transition from a kinematic to a dynamical regime is indicated by the decreasing slope of the curve in figure 2(*a*), as V^* approaches its maximum value V_m. The change can also be seen by inspecting the detailed solutions. In the kinematic regime $|u|$ rises linearly from the boundaries and the field has a Gaussian profile in the flux sheets, while the vorticity pattern has a single central peak, as in figure 4(*a*) of I. Once $V_0 \geqslant 70$, the vorticity changes sign in the current sheets and motion is gradually excluded from

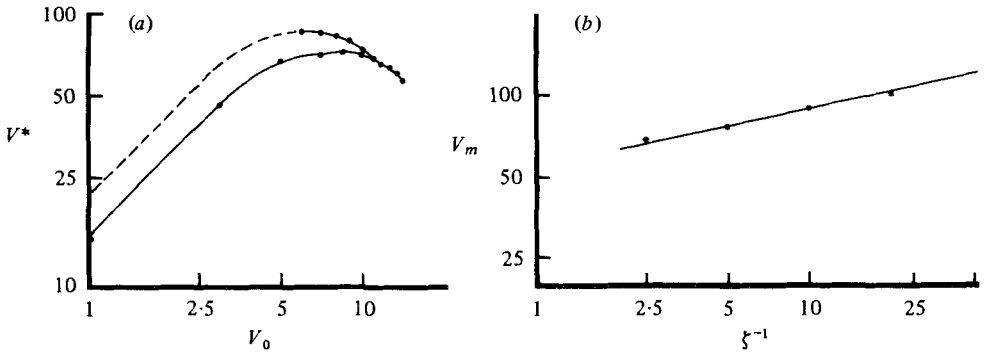

FIGURE 2. The transition from a dynamical to a kinematic regime. (*a*) Variation of peak field with average field: V^* as a function of V_0 for $\zeta = 0{\cdot}2$ and $\zeta = 0{\cdot}1$. The broken line for $\zeta = 0{\cdot}1$ is fitted to the kinematic solution derived from that for $\zeta = 0{\cdot}2$. (*b*) Variation of the maximum field strength V_m with ζ^{-1}.

regions with strong fields until, for $Q \approx Q_{\max}$, the field structure resembles that in figure 4(*b*). Indeed, the transverse velocity within the flux sheets is already substantially reduced when V^* reaches a maximum.

Results obtained when $\zeta = 0{\cdot}1$ are also shown in figure 2(*a*). From the values given in table 1 it can be seen that $Q_{\max}$ is independent of ζ and that $Q_{\max}$ is marginally greater than $Q^{(i)}$, as expected from I. For $Q < Q_{\max}$ the amplified field V^* is at first independent of ζ but goes on increasing longer with decreasing Q when $\zeta = 0{\cdot}1$, so that the maximum value V_m is higher than that for $\zeta = 0{\cdot}2$, and occurs at a lower value of V_0. A few runs were also carried out with $\zeta = 0{\cdot}4$ and $\zeta = 0{\cdot}05$ in order to obtain the corresponding values of V_m, though the dynamical regime did not develop fully in the former case. The maximum fields are plotted logarithmically against the reciprocal of ζ in figure 2(*b*). The points can be fitted by a straight line such that

$$V_m \propto \zeta^{-0{\cdot}20} \tag{2.6}$$

for $\zeta \lesssim 0{\cdot}3$. The transition from the kinematic to the dynamical regime has been studied in greater detail by Peckover & Weiss (1978) who obtained an almost identical power law for Oberbeck magnetoconvection. (In dimensional terms (2.6) implies that $B_m \propto \eta^{-0{\cdot}2}$: for a given R the maximum field attainable in a flux sheet increases without limit as $\eta \to 0$.)

Simple physical arguments suggest that this transition occurs when $R_m \sim Q^2$ (equation I(7.4)). Since $U \sim R^{2/3}$ when $R \gg R_0$ (Moore & Weiss 1973), the kinematic regime should extend over the range $Q < Q_m \sim \zeta^{-\frac{1}{2}} R^{-\frac{1}{3}}$ (Galloway *et al.* 1978). The numerical results can be fitted if $\zeta^{\frac{1}{2}} Q_m \approx 130$. For a given Rayleigh number, V^* should reach a maximum around the transition from the kinematic to the dynamical regime, where $V^* = V_m$ and

$$V_m \sim R^{\frac{1}{2}} \zeta^{-\frac{1}{4}} \tag{2.7}$$

(Galloway *et al.* 1978). The exponent of ζ in (2.7) is not too far from that in (2.6), which was derived from the numerical experiments.

Unfortunately, the dynamical range in figures 1 and 2(*a*) is not wide enough to establish the existence of any asymptotic regime. The appropriate parts of the curves in figure 1 can be fitted by setting $N \propto Q^{-\frac{1}{2}}$. This, combined with the results in I,

suggests that the Nusselt number might be given by an expression of the form

$$N = (R/\zeta Q)^{\frac{1}{2}} f(\zeta), \tag{2.8}$$

where $f(\zeta)$ is a slowly varying function that increases with ζ.

3. Spatially asymmetrical motion

The solutions of the differential equations I(2.12)–I(2.15) can be expanded in Fourier series of the form

$$\psi(x,z,t) = \sum_m \sum_n \Psi_{mn}(t) \sin(m\pi x/\lambda) \sin n\pi z. \tag{3.1}$$

The fundamental mode for the linear problem, and all higher-order terms generated by perturbing about the static solution, have the property that

$$\Psi_{mn} = 0 \quad (m+n \text{ odd}). \tag{3.2}$$

Furthermore, it can be shown (cf. Veronis 1966) that, if the initial values satisfy (3.2), then this condition will be satisfied for all subsequent times. The solutions then possess symmetry about the point $(\frac{1}{2}\lambda, \frac{1}{2})$ and this symmetry is preserved by the finite-difference schemes provided that N_x, N_z are both even. The equations are, however, solved numerically over the whole region $\{0 < x < \lambda;\ 0 < z < 1\}$ and the symmetry may be violated owing to the effect of rounding errors. In fact, the contours displayed in I are symmetrical about the centre of the cell and this property provides a useful check on the accuracy of the computations.

It is still possible that solutions satisfying (3.2) may be unstable to small disturbances with $(m+n)$ odd, and that these perturbations may grow until they eventually destroy the symmetry of the nonlinear solutions. In some numerical experiments such instabilities did indeed develop. Careful inspection of the results in I shows that, when the vorticity is all of one sign and the flux sheets retain a Gaussian profile, the solutions remain almost perfectly symmetrical and any asymmetry gradually decays. In runs with dynamically active flux sheets, from which the motion is excluded, the solutions behave differently. In the examples with $\zeta Q = 100$, $\lambda = 1$ and $\zeta \leqslant 0{\cdot}2$, the rounding error introduced perturbations with $(m+n)$ odd and these perturbations grew, nearly exponentially, on a slow diffusive timescale. When the disturbance became large ($\sim 20\,\%$) it developed faster and the solutions became time-dependent before eventually attaining a new, asymmetric steady state.

The same effect occurs in runs with $R = 10^4$ and $\lambda = 1$, as Q approaches $Q_{\max}$ from below (for example with $\zeta = 0{\cdot}2$, $700 \leqslant Q \leqslant 1000$ and $\zeta = 0{\cdot}1$, $100 \leqslant Q \leqslant 1960$). In this regime small perturbations to the static, conducting solution develop into large-amplitude, symmetrical convection which is apparently steady (like the solutions discussed in §2). Then a gradual transfer of magnetic flux across the cell leads to a different steady state. In this alternative solution most of the flux is concentrated on one side of the cell, which acquires a lopsided appearance, as shown in figure 3. Here a broad sheet, containing 90% of the total flux, occupies about one-third of the cell, while the eddy is confined to the remaining two-thirds. This flux sheet is almost stagnant, apart from a weak counterflow driven by the inclined isotherms. Which side the sheet appears on, like the sense of the motion, is determined by the initial

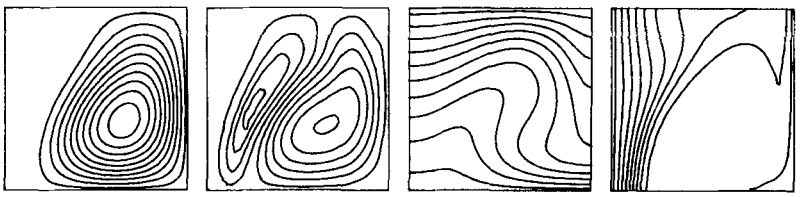

FIGURE 3. Spatially asymmetrical convection. Contours of ψ (streamlines), ω, T (isotherms) and A (lines of force) for $R = 10^4$, $Q = 1210$, $\zeta = 0{\cdot}1$.

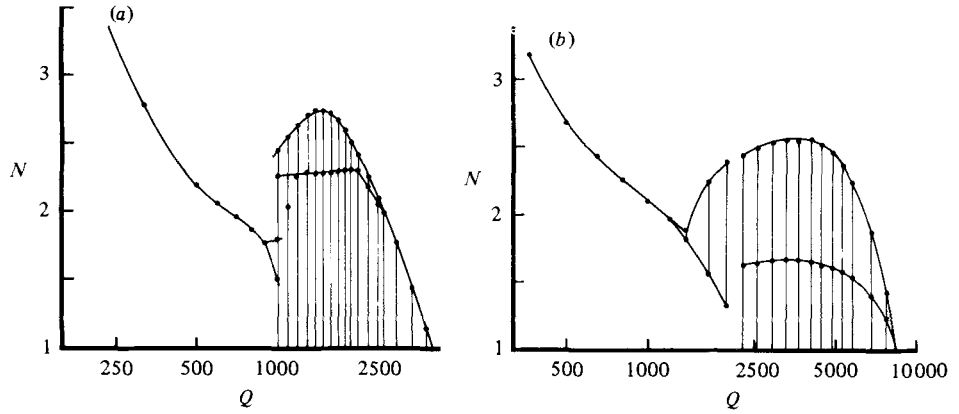

FIGURE 4. Spatially asymmetrical solutions. Variation of N with Q for (*a*) $\zeta = 0{\cdot}2$, (*b*) $\zeta = 0{\cdot}0$. The maximum extent of oscillations about the steady state is shown, together with the different maxima for oscillations with reversal of the main flow.

conditions. The numerical results show no preference for any of the four possible orientations. The solution shown in figure 3 was confirmed by stretching the mesh from 24 to 48 intervals: this change affected the amount of flux in the sheet by less than 0·2 %. As a further check, the average values of B_z at the left- and right-hand boundaries were compared. It can readily be proved, by integrating I(2.13) over the region, that in a steady state these average values must be equal (Proctor & Weiss 1978). The numerical results satisfy this constraint within limits set by the truncation error.

The lopsided solutions persist throughout the dynamical regime both for $\zeta = 0{\cdot}2$ and for $\zeta = 0{\cdot}1$. As Q is decreased the asymmetry gradually declines until it disappears, inevitably, in the kinematic regime. The variation of N with Q is shown in figure 4: throughout the range $Q_m < Q < Q_{\max}$, the Nusselt numbers for the spatially asymmetrical solutions were slightly less than those for the symmetric solutions, as can be seen from the appendix. Nevertheless, the former were preferred. This behaviour can be explained as follows. At the edge of a dynamically active flux sheet, both the normal and the tangential component of the velocity are small. The formation of a single large flux sheet at one side of the cell allows the effective boundary condition on the other side to be relaxed. The tangential velocity vanishes on one side only, while a healthy thermal plume forms at the other. Convection therefore becomes more vigorous in the field-free region (for the case in figure 3, the peak velocity is 50 % greater and the kinetic energy is up by 20 %). On the other hand, the single flux sheet occupies a larger proportion of the region (the peak field and the magnetic energy are down by 30 % and 25% respectively) and so the total heat transport is actually

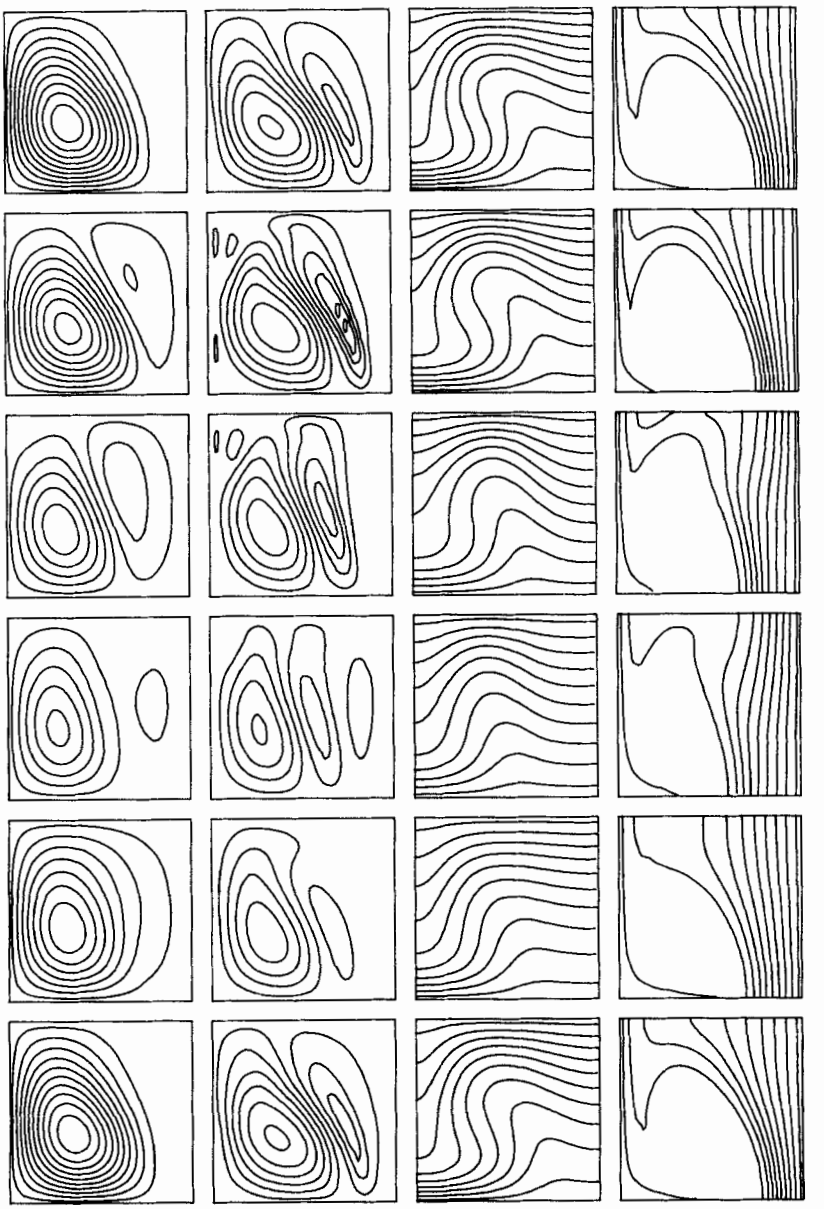

FIGURE 5. Asymmetrical oscillations without reversal of the main flow. Contours of ψ, ω, T and A at six equally spaced intervals of time during a cycle for $Q = 1960$, $\zeta = 0{\cdot}1$. The contour levels remain fixed throughout the sequence.

reduced. The same physical picture also explains the development of the instability, for, if a little flux is peeled off one side, then convection speeds up on that side: hence more flux is carried across the cell and the asymmetry is enhanced.

As Q is gradually increased the solutions become time-dependent. For $Q < Q_{\max}$, computed in §2 above, the sense of motion in the main convective eddy does not change. Within the flux sheet, however, there are periodic oscillations. The changing

patterns of the velocity, vorticity, temperature and magnetic field are illustrated in figure 5. The sense of motion in the subsidiary cell is alternately identical with and opposite to that in the main eddy. As a result the main flow is modulated with the same frequency and the Nusselt number also varies, with the same period as the velocity. At any level $N(z)$ oscillates regularly between its maximum and minimum values: for the orientation shown in figure 5, the range of variation in N is greater at $z = 0$, where the sheet is compressed, than at $z = 1$. This range is indicated in figure 4. Similar oscillations have been described for convection in a cylindrical cell by Galloway (1978) and Galloway & Moore (1979). As they point out, the effective values of Q are different in the magnetic and nonmagnetic regions. Thus it is possible for overstable convection to develop in the flux sheet and to coexist with steady motion in the rest of the cell. The whole flow then oscillates without reversing the sense of motion in the main eddy.

As Q is increased these oscillations grow more vigorous, cf. figure 4(*b*). Eventually they give way to a different kind of oscillation, in which the main eddy reverses during the cycle, while the flux sheet undergoes varicose pulsations. Contours of ψ, ω, T and A for half the cycle with $\zeta = 0{\cdot}1$, $Q = 2890$ are displayed in figure 6. The countercell swells until the main cell is extinguished and the sense of motion is reversed. The corresponding variation in the Nusselt number is shown in figure 7(*a*). $N(0)$ is greatest at about the time of the first set of contours; its value falls almost to unity as the flow is halted, and then rises to a lesser maximum near the last set of contours. Thereafter it drops to a subsidiary minimum before rising to its initial value. $N(1)$ behaves identically except for a phase difference of 180°.

This pattern persists throughout the oscillatory regime. Both maxima are shown in figure 3. For $\zeta = 0{\cdot}2$, the lesser maximum, N_2, does not vary significantly over a wide range of Q. The greater maximum, N_1, rises to a peak and then falls toward N_2. For $Q \gtrsim 2500$ the oscillations are effectively symmetrical and $N_1 \approx N_2$. When $\zeta = 0{\cdot}1$, N_1 and N_2 approach each other as $Q \to Q^{(o)}$. For Q slightly greater than $Q^{(o)}$, cells with $\lambda = \frac{1}{2}$ are still overstable and the oscillations break up into two (unequal) cells.

As Q is decreased, the period of the asymmetrical oscillations increases monotonically, rising sharply when Q approaches $Q_{\max}$, as shown in figure 7(*b*). A plausible conjecture is that the different types of oscillations in figures 3(*a*) and (*b*) belong to the same solution branch. If so, they must be linked by an unstable portion of that branch, since both types can be present at the same value of Q. The transition from oscillations in which the flow does not reverse to oscillations with reversal of the motion then takes place via a singular oscillation with infinite period, in which the velocity just reaches zero (cf. Knobloch & Proctor 1981).

The same pattern of behaviour was found for axisymmetric convection by Galloway & Moore (1979), though the geometrical distinction between the axis and periphery of a cell makes any asymmetry harder to discern. The hysteresis in figure 11 of their paper seems to be related to the appearance of spatially asymmetric solutions, with different types of oscillation like those described here. The transition from symmetrical oscillations, like those in figure 8 of I, to spatially asymmetrical solutions, like those in figure 6, leads to an apparent doubling of period in N, as N_1 and N_2 diverge. This is quite distinct from the bifurcation discussed in I, which led to temporally asymmetrical solutions (see also Knobloch, Weiss & Da Costa 1981), that retained their symmetry in space.

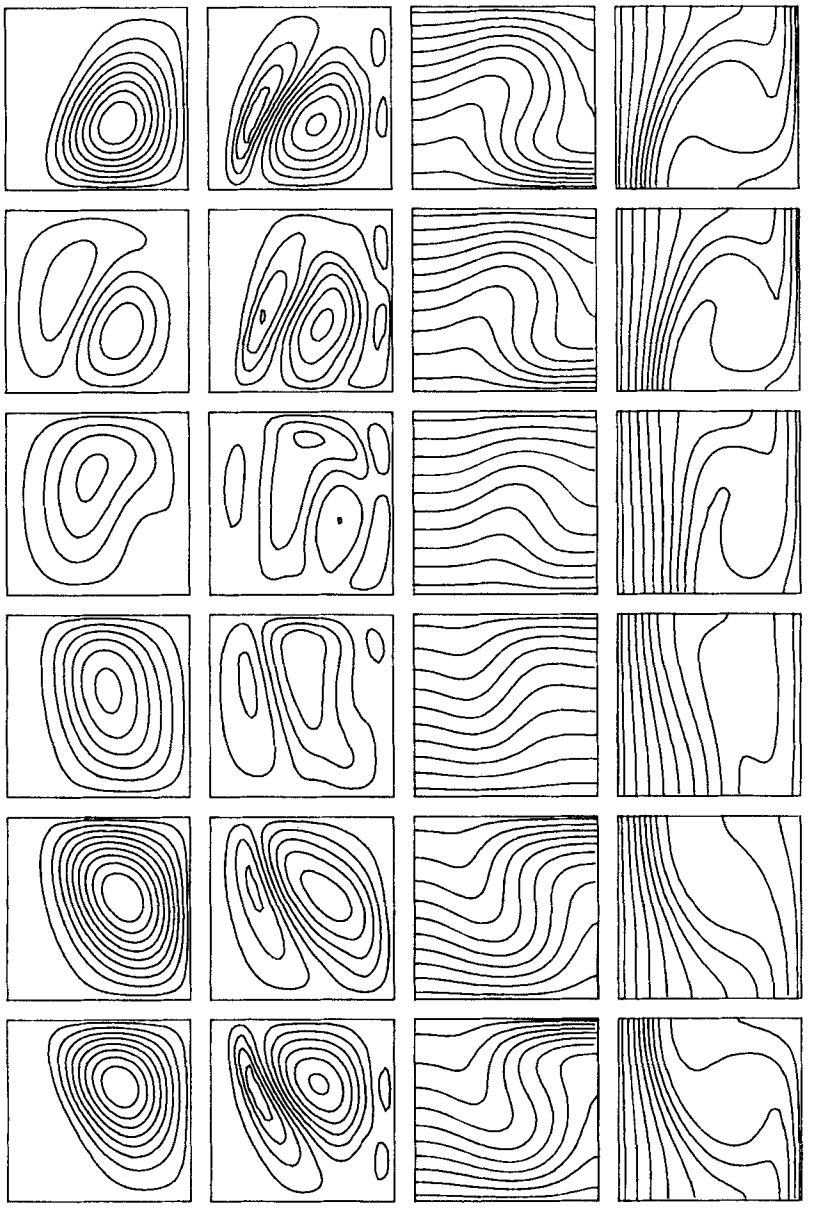

FIGURE 6. Asymmetrical oscillations with reversal of the motion. As for figure 5, but for a half-cycle only, with $Q = 2890$.

4. The horizontal scale of convection

The results in the previous section demonstrated a preference for asymmetrical plan forms in square cells ($\lambda = 1$). In this section the effect of varying the cell width λ will be investigated. In an infinite layer λ can vary continuously and for any configuration a preferred scale should eventually emerge; in numerical experiments we are restricted to discrete values of λ. Linear theory implies that for large R narrow cells

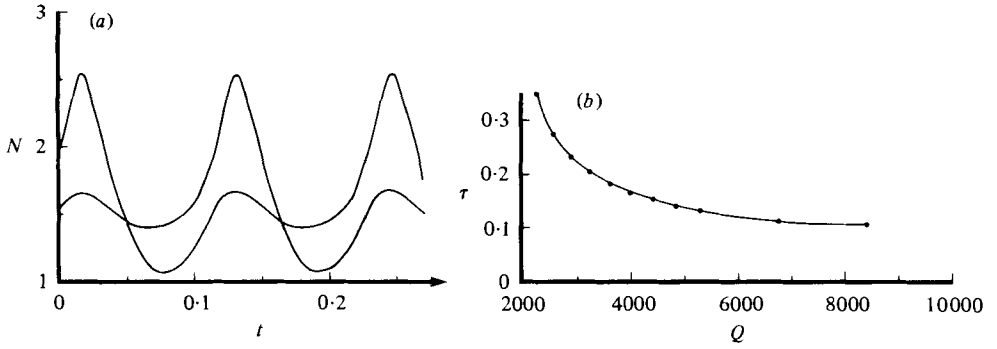

FIGURE 7. Asymmetrical oscillations. (*a*) $N(0)$ and $N(1)$ as functions of time for the case in figure 6. N is greatest where the sheet is most compressed. (*b*) Variation of the period P with Q for $\zeta = 0{\cdot}1$.

λ	$Q^{(o)}$	$Q^{(i)}$	$Q^{(e)}$	$Q_{\max}$
$\frac{1}{3}$		stable		
$\frac{1}{2}$	3794	765	564	—
1	3748	1055	467	1050
2	1504	426	187	3200

TABLE 2. The effect of varying the cell width ($R = 10^4$, $\zeta = 0{\cdot}2$).

are preferred: for example, $Q^{(e)}$ is a maximum when

$$\lambda = [(R/2\pi^4)^{\frac{1}{3}} - 1]^{-\frac{1}{2}}. \tag{4.1}$$

Thus, for $R = 10^4$, $Q^{(e)}$ attains its maximum value of 604 when $\lambda \approx 0{\cdot}607$. Table 2 shows the effect of varying λ when $\zeta = 0{\cdot}2$. The critical values of Q for $\lambda = \frac{1}{2}$ and $\lambda = 1$ differ only slightly and square cells showed no tendency to break in two. (With $\zeta = 0{\cdot}1$, the square cell did split into two oscillating cells when Q was slightly less than $Q^{(o)}$.) According to linear theory, cells with $\lambda = 2$ are much more stable than those with $\lambda = 1$.

Things are different in the nonlinear regime. In an attempt to discover the preferred horizontal scale several runs were started with 'noisy' initial conditions, obtained by adding to the static solution a temperature perturbation proportional to

$$\sum_{m=1}^{6} \cos(m\pi x/\lambda).$$

A test run with $Q = 0$, $\lambda = 2$ yielded two nearly symmetrical cells; this was followed by a series with $Q = 800$, $\zeta = 0{\cdot}2$ and $\lambda = 2, 3, 4$. The run with $\lambda = 2$ generated an initially complicated flow which rapidly developed into a single, slightly asymmetric cell. With $\lambda = 3$, two similar cells appeared, with opposite senses of rotation. One of these cells then grew at the expense of the other until it eventually occupied about 60 % of the region. When $\lambda = 4$ there were three cells at first, but the solution eventually settled down to give two more or less equal cells, rotating in the *same* sense (see figure 3 of Galloway & Weiss 1981). It seems, therefore, that in the dynamical regime relatively flat cells, with $\lambda \approx 2$, are favoured.

The preference for flat cells extended over a wide range in Q. Figure 8 shows streamlines and lines of force for steady solutions with $\zeta = 0{\cdot}2$, $\lambda = 2$ as Q is increased. The

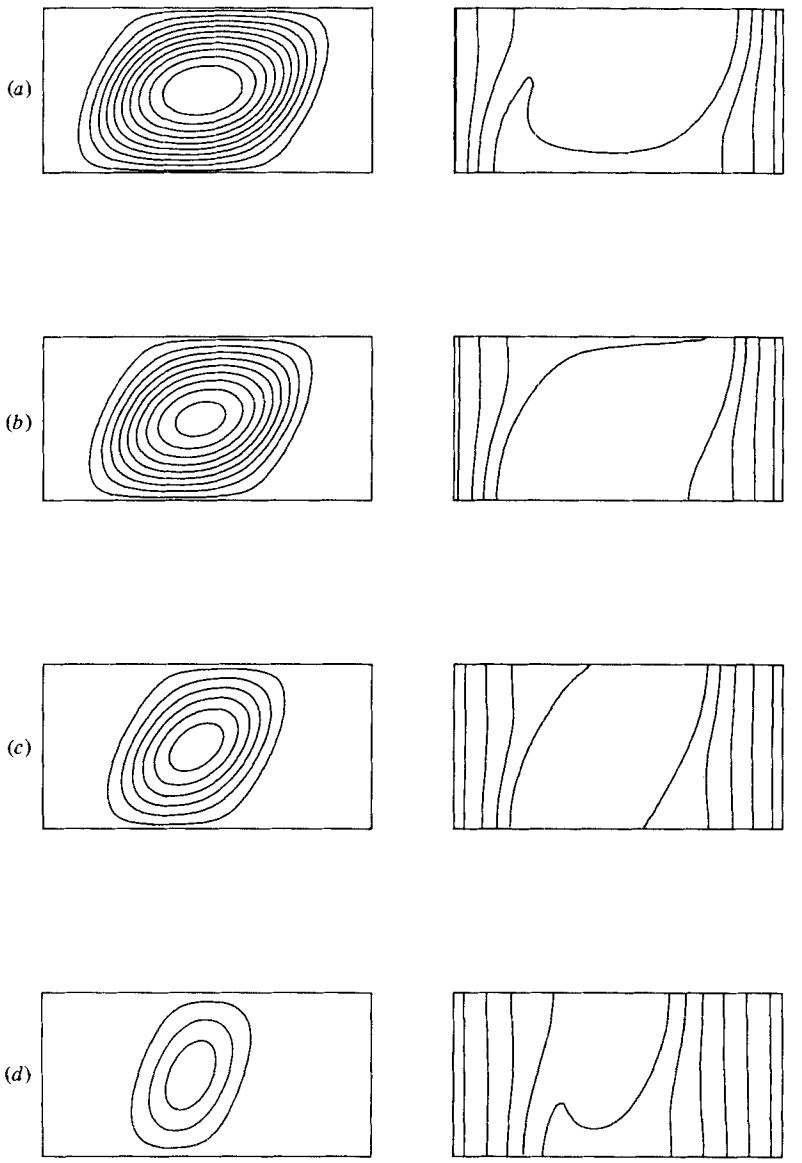

FIGURE 8. Convection in flat cells. Streamlines and lines of force for $\lambda = 2$ and $\zeta = 0{\cdot}2$, and (*a*) $Q = 1000$, (*b*) $Q = 1400$, (*c*) $Q = 1900$, (*d*) $Q = 2300$. The contour levels are the same for all four values of Q.

flow is slightly asymmetrical and magnetic flux is confined to thick sheets from which the motion is excluded. As Q becomes larger these sheets expand and the convective eddy shrinks: for $Q = 2300$, it only occupies 40 % of the region and the rest is virtually stagnant. When $Q = 2400$ steady convection gives way to irregular small-scale oscillations. In figure 9, N is plotted against Q for cells with $\lambda = 2$ and $\lambda = 1$. Throughout the dynamical range, N is larger for $\lambda = 2$. Only in the kinematic regime, for $Q \lesssim 200$, does N become larger for square cells. Moreover, steady convection is possible for much higher values of Q when $\lambda = 2$, despite the predictions of linear

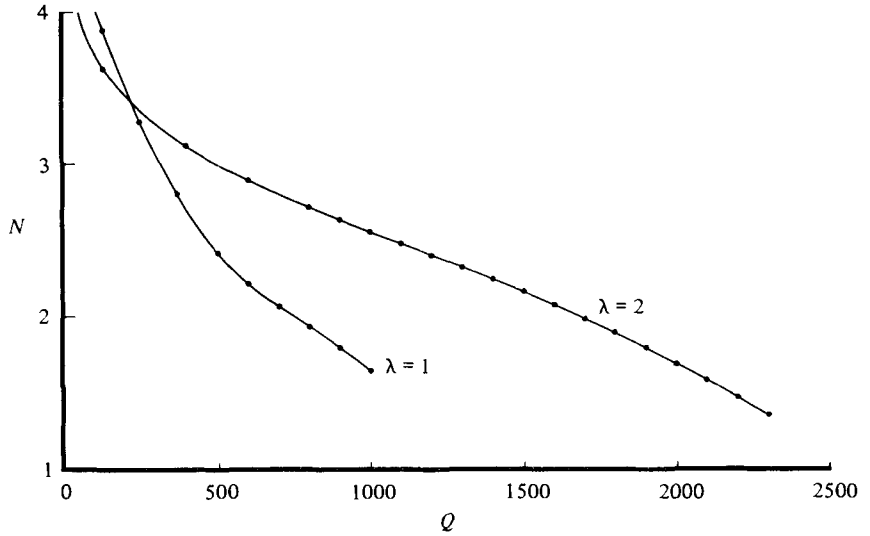

FIGURE 9. Subcritical convection in flat cells: N as a function of Q for $\zeta = 0{\cdot}2$, and $\lambda = 1, 2$. Note that, unlike figure 1, Q varies linearly here.

theory. Indeed, steady solutions exist beyond the range of linear instability since, for $\lambda = 2$, $Q_{\max} > Q^{(o)}$.

For two-dimensional convection in the absence of a magnetic field, N is greatest, at this value of R, when $\lambda \approx \sqrt{2}$ (Fromm 1965; Veronis 1966; Moore & Weiss 1973). In the presence of a strong field, the preferred horizontal scale is rather wider, around $\lambda = 2$. As figure 8 shows, magnetic flux is pushed aside, leaving a field-free region in which convection can take place. The effective value of λ for this field-free region is then in the range $1 \lesssim \lambda \lesssim 1{\cdot}5$, as might be expected. In order to accommodate both the motion and the stagnant slab of flux, wide cells are favoured in the nonlinear regime.

5. Conclusion

Spatially symmetrical solutions have been followed through from the onset of convection to the kinematic regime. The onset of overstability and the transition from oscillatory to steady motion have already been described in I. The results in §4 suggest that, despite inferences from linear theory, steady convection first occurs in cells with widths of order unity. For these cells, $Q_{\max}$ may be much greater than $Q^{(e)}$ (or $R_{\min}$ much less than $R^{(o)}$), as in the simplified model of Knobloch *et al.* (1981). Symmetrical solutions can be maintained by explicitly imposing the symmetry condition (Veronis 1966; Moore & Weiss 1973) but in practice asymmetrical instabilities grow so slowly that it is not difficult to obtain almost perfectly symmetrical results.

In the dynamical regime these instabilities do eventually become important and lopsided cells, like that in figure 3, are preferred. The numerical experiments show that the branch of steady, symmetrical solutions is unstable, but it is not obvious that there exists a finite value of Q at which the bifurcation to asymmetry takes place. The

transition from steady to oscillatory motion on the asymmetrical branch differs from that covered in I and discussed by Knobloch *et al.* (1981). Instead, there is first a bifurcation to periodic solutions in which the sense of the main eddy does not change. The amplitude of the oscillations then increases until there is a transition to oscillations in which the motion reverses, via a critical solution with infinite period. The asymmetry is reduced as Q approaches $Q^{(o)}$, but it is again unclear whether there is an actual bifurcation at some $Q < Q^{(o)}$.

A physical explanation of the development of lopsided solutions was given in §3. In the dynamical regime a symmetrical convective eddy is sandwiched between stagnant sheets of flux, which effectively change the lateral boundary conditions so that the tangential velocity vanishes instead of the tangential stress. Transferring most of the flux to one side of the cell allows the boundary condition on the other side to be relaxed, so that convection proceeds more vigorously in the field-free region (cf. figure 3). The formation of flux sheets is encouraged by the presence of boundaries on which $u = 0$. However, a run with $\lambda = 4$ produced two lopsided cells, with the principal flux concentration in the centre, away from the lateral boundaries (Galloway & Weiss 1981). Thus the preference for asymmetrical cells cannot be ascribed to the rather artificial choice of periodic boundary conditions.

The computations described here were designed to yield regular solutions that were either steady or strictly periodic. At higher Rayleigh numbers time-dependent behaviour is more common and also more erratic. Runs with $R = 10^5$ are consequently more difficult to interpret (Weiss 1981*b*), and at larger Rayleigh numbers the finite-difference schemes become inaccurate. In any case, idealized two-dimensional models become rather unrealistic at high Rayleigh numbers. In the absence of a magnetic field two-dimensional rolls become unstable and dynamically active flux sheets are probably unstable to varicose modes that lead to the formation of isolated tubes or ropes (Galloway & Weiss 1981).

Nevertheless, one may conclude that nonlinear magnetoconvection favours intermittent structures. When the average field is strong there may be isolated convective eddies in regions where the field is locally reduced, as in figure 8(*d*). For weaker average fields, magnetic flux tends to be confined to ropes from which the motion is excluded and eventually, in the kinematic limit, flux concentration is limited only by diffusion. The preference for spatially asymmetrical solutions in the nonlinear regime suggests that in an extensive layer convection may assemble magnetic flux into a few large ropes, leaving the rest of the region almost field-free (Galloway & Weiss 1981). Moreover, magnetic fields are likely to be intermittent in any turbulent fluid when the magnetic Reynolds number is large (cf. Orszag & Tang 1979).

All these arguments imply that fields in stellar convective zones should be confined to isolated tubes. This is true both of magnetic fields in the photospheric network on the sun (Harvey 1977; Stenflo 1977) and of flux emerging through its surface (Golub *et al.* 1980). Any description of the generation of magnetic fields within convective zones should therefore take account of this complicated intermittent structure. Further progress in studying turbulent magnetic fields requires models that include the effect of three-dimensionality, magnetic buoyancy and compressibility, and it is with these that future work will be concerned.

I am very grateful to Dr J. M. Wheeler for assistance with most of the runs described

here. Computation was carried out on the IBM 360/44 at the Institute of Theoretical Astronomy and the 370/165 of the University Computing Service. I thank N.J. Butler, L.N. Da Costa, D.J. Galloway, D.O. Gough, E. Knobloch, D.R. Moore, R.S. Peckover, M.R.E. Proctor and H.U. Schmidt for suggestions and encouragement. This research was supported by the Science Research Council and the paper was begun at the Harvard–Smithsonian Center for Astrophysics.

Appendix

The list below specifies details of over 120 numerical experiments whose results are included in this paper. In each case $R = 10^4$ and $\sigma = 1$; $N_x = 24$ unless stated otherwise. Values of Q are followed by corresponding values of the Nusselt number in brackets. Symmetrical solutions are listed first: the light-face figures indicate the maximum and average values of N for oscillations and the bold-face figures are for steady convection. For the spatially asymmetrical solutions, light-face figures indicate the two maxima of N for oscillations with reversal of the main flow; bold-face figures give values of N for steady convection or, where appropriate, the maximum and minimum values for oscillations without reversals of the main flow. An asterisk denotes a run with perceptible asymmetry and a dagger denotes solutions in which the vorticity does not change sign at the edges of the flux sheets. The symbol *s* indicates that a run started from the last oscillatory solution settled down to motion without reversals of direction in the main eddy; **o** indicates that a run started from a steady (or non-reversing) solution developed oscillations with reversals.

(*a*) *Symmetrical solutions* ($\lambda = 1$)

$\zeta = 0{\cdot}4$, 300 (**2·36***), 275 (**2·56**), 250 (**2·79**), 202 (**3·04**)

$\zeta = 0{\cdot}2$, 3920 (**1**), 3600 (1·14, 1·07), 3200 (1·43, 1·21), 3125 (1·49, 1·23), 2800 (1·74, 1·36), 2500 (1·99, 1·48), 2400 (2·07, 1·53*), 2200 (2·21, 1·60*), 2000 (2·43, 1·70*), 1700 (2·54, 1·75*), 1400 (2·60, 1·78*), 1100 (2·4, 1·60*; **o**), 1000 (2·35, 1·41; **1·63***), 900 (*s*; **1·79***), 800 (**1·92***), 700 (**2·07***), 600 (**2·22**), 500 (**2·42**), 361 (**2·79**), 245 (**3·28**), 361 (**2·79**), 245 (**3·28**); $N_x = 48$: 125 (**3·88**†), 45 (**4·53**†), 5 (**4·92**†).

$\zeta = 0{\cdot}1$, 7840 (1·21, 1·14, 2 cells), 6760 (1·48, 1·28*), 5760 (1·98, 1·47*), 4000 (2·53, 1·82*), 3240 (2·65, 1·85*), 2560 (2·40, 1·72*), 2250 (2·43, 1·71*; **o**), 1960 (2·26, 1·42; **1·58***), 1690 (*s*; **1·75***), 1440 (**1·89***), 1210 (**2·05***), 1000 (**2·20**); $N_x = 48$: 810 (**2·37**), 640 (**2·60**), 490 (**2·87**), 360 (**3·19**).

$\zeta = 0{\cdot}05$, $N_x = 48$: 720 (**2·92**), 500 (**3·28**).

(*b*) *Asymmetrical solutions* ($\lambda = 1$)

$\zeta = 0{\cdot}2$, 3600 (1·14, 1·14), 3200 (1·43, 1·43), 2800 (1·74, 1·74), 2500 (1·99, 1·88), 2400 (2·08, 2·05), 2200 (2·25, 2·18), 2000 (2·42, 2·29),

1900 (2·51, 2·30), 1800 (2·60, 2·30), 1700 (2·67, 2·29), 1600 (2·72, 2·28), 1500 (2·74, 2·27), 1400 (2·74, 2·27), 1300 (2·71, 2·28), 1200 (2·64, 2·26), 1100 (2·56, 2·18; o), 1000 (2·45, 2·26; **1·76**, **1·56**), 900 (*s*; **1·77**), 800 (**1·86**), 700 (**1·96**), 600 (**2·06**), 500 (**2·19**), 320 (**2·78**), 180 (**3·58**); $N_x = 48$: 700 (**1·96**).

$\zeta = 0{\cdot}1$, 8410 (1·14, 2 cells), 7840 (1·43, 1·25), 6760 (1·87, 1·40), 5760 (2·25, 1·54), 5290 (2·38, 1·58), 4840 (2·47, 1·61), 4410 (2·53, 1·63), 4000 (2·57, 1·66), 3610 (2·57, 1·67), 3240 (2·56, 1·67), 2890 (2·54, 1·66), 2560 (2·49, 1·64), 2250 (2·45, 1·63; o), 1960 (*s*; **2·41**, **1·34**), 1960 (**2·25**, **1·55**), 1440 (**1·92**, **1·81**), 1210 (**1·97**), 1000 (**2·10**), 810 (**2·26**), 640 (**2·44**), 490 (**2·69**), 360 (**3·26**); $N_x = 48$: 1000 (**2·12**).

(*c*) *Flat cells* ($\lambda = 2$, $N_x = 48$)

$\zeta = 0{\cdot}2$, 2400 (o), 2300 (**1·35**), 2200 (**1·47**), 2100 (**1·58**), 2000 (**1·68**), 1900 (**1·80**), 1800 (**1·91**), 1700 (**1·98**), 1600 (**2·07**), 1500 (**2·17**), 1400 (**2·25**), 1300 (**2·32**), 1200 (**2·39**), 1100 (**2·48**), 1000 (**2·56**), 900 (**2·64**), 800 (**2·72**), 600 (**2·90**), 400 (**3·10**), 125 (**3·63**), 0 (**4·66**).

REFERENCES

Cowling, T. G. 1976 *Magnetohydrodynamics*. Bristol: Hilger.

Fromm, J. E. 1965 Numerical solutions of the nonlinear equations for a heated fluid layer. *Phys. Fluids* **8**, 1757–1769.

Galloway, D. J. 1978 The origin of running penumbral waves. *Mon. Not. Roy. Astr. Soc.* **184**, 49P–52P.

Galloway, D. J. & Moore, D. R. 1979 Axisymmetric convection in the presence of a magnetic field. *Geophys. Astrophys. Fluid Dyn.* **12**, 73–106.

Galloway, D. J., Proctor, M. R. E. & Weiss, N. O. 1978 Magnetic flux ropes and convection. *J. Fluid Mech.* **87**, 243–261.

Galloway, D. J. & Weiss, N. O. 1981 Convection and magnetic fields in stars. *Astrophys. J.* **243**, 945–953.

Golub, L., Rosner, R., Vaiana, G. S. & Weiss, N. O. 1981 Solar magnetic fields: the generation of emerging flux. *Astrophys. J.* **243**, 309–316.

Harvey, J. W. 1977 Observations of small-scale magnetic fields. *Highlights of Astronomy* **4**, part II, 223–239.

Knobloch, E. & Proctor, M. R. E. 1981 Nonlinear periodic convection in double-diffusive systems. *J. Fluid Mech.* **108**, 291–316.

Knobloch, E., Weiss, N. O. & Da Costa, L. N. 1981 Oscillatory and steady convection in a magnetic field. *J. Fluid Mech.* (submitted).

Moore, D. R. & Weiss, N. O. 1973 Two-dimensional Rayleigh–Bénard convection. *J. Fluid Mech.* **58**, 289–312.

Orszag, S. A. & Tang, C.-M. 1979 Small-scale structure of two-dimensional magnetohydrodynamic turbulence. *J. Fluid Mech.* **90**, 129–143.

Peckover, R. S. & Weiss, N. O. 1978 On the dynamic interaction between magnetic fields and convection. *Mon. Not. Roy. Astr. Soc.* **182**, 189–208.

Proctor, M. R. E. & Weiss, N. O. 1978 Magnetic flux ropes. *Rotating Fluids in Geophysics* (ed. P. H. Roberts and A. M. Soward), pp. 389–408. Academic.

STENFLO, J. O. 1977 Influence of magnetic fields on solar hydrodynamics: experimental results. *I.A.U. Colloquium no.* 36 (ed. R. M. Bonnet & P. Delache), pp. 143–188. Clermont-Ferrand: de Bussac.

VERONIS, G. 1966 Large-amplitude Bénard convection. *J. Fluid Mech.* **26**, 49–68.

WEISS, N. O. 1981*a* Convection in an imposed magnetic field. Part 1. The development of nonlinear convection. *J. Fluid Mech.* **108**, 247–272.

WEISS, N. O. 1981*b* The interplay between magnetic fields and convection. *J. Geophys. Res.* (submitted).